Rock Mechanics
and Rock Engineering 16, 253—274 (1983)

**Rock Mechanics
and Rock Engineering**

Numerical Simulation of Rock Burst Processes Treated as Problems of Dynamic Instability

By

A. Zubelewicz and Z. Mróz

Institute of Fundamental Technological Research, Warsaw, Poland

Summary

The phenomenon of rock burst occurs when the static stability conditions of the rock mass are violated and the dynamic failure process proceeds starting from the equilibrium state. In view of the difficulties in determining numerically the instability point, an alternative approach is advocated here: after solving the initial static problem the mode and onset of dynamic failure are studied by superposition of dynamic disturbances. In this way quantitative analyses of rock burst phenomena may be handled in a relatively simple manner.

1. Introduction

The phenomenon of rock burst occurs when static stability conditions of rock mass are violated and the uncontrollable dynamic failure process proceeds starting from the equilibrium state. A portion of rock mass is then usually in the damaged state represented by the unstable branch of the stress-strain relation, whereas the remaining portion is in the elastic or elasto-plastic hardening state. The stability conditions for the rock excavations were discussed in general terms by Petukchov and Linkov (1979), and the stability of a set of pillars was considered by Salamon (1970), and Crouch and Fairhurst (1974). The mechanisms of dynamic fracture of rock were analysed by Bieniawski (1968) and Burgert and Lippmann (1981).

Although it is fairly easy to derive stability conditions, the numerical determination of the instability point is rather difficult in view of the necessity of incremental static analysis for varying geometric parameters of excavation. An alternative dynamic approach seems more effective in this case. In fact, assuming this approach, the study is made of a subsequent motion following the dynamic disturbance superposed upon the initial equilibrium state. At the instability point, the small initial disturbance is greatly amplified and the whole dynamic failure process can be numerically studied by departing from an initial state close to the instability point. The aim of this paper is to apply the dynamic approach in the study of rock burst processes.

0723-2632/83/0016/0253/$ 04.40

In Section 2 the stability and instability conditions will be briefly discussed and the problem formulation will be presented. In Section 3 the numerical procedure and the type of finite elements used in our study will be described. Finally, in Section 4 the instability conditions and the modes of failure of one or several pillars will be studied numerically.

2. Instability Conditions and Modes of Failure

Fig. 1a presents schematically the typical stress-strain diagram of a rock material under uniaxial compression and tension. After reaching the maximum stress values σ_c or σ_t in compression or tension, the material exhibits unstable post-critical response, usually accompanied by a localized deformation along shear bands or by opening and propagation of cracks. The residual

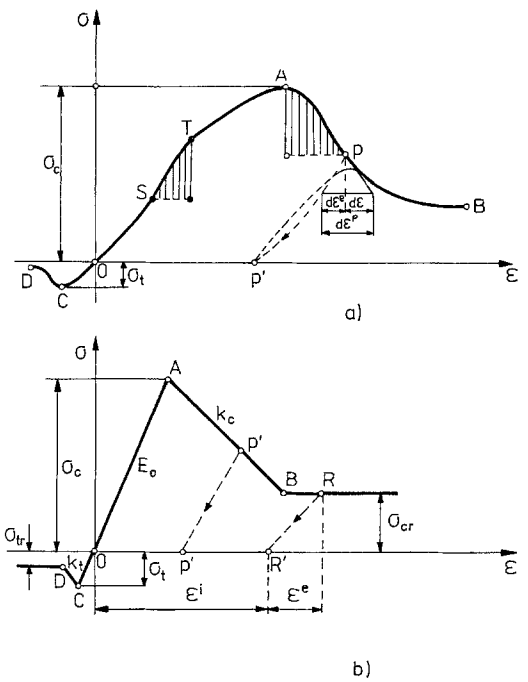

Fig. 1. a) Typical stress-strain diagram for rock; b) simplified piece-wise linear diagram

stress σ_r in compression corresponds to frictional resistance of broken material when the lateral pressure is applied to the specimen. Fig. 1b presents a simplified diagram composed of linear portions exhibiting characteristic values σ_c, σ_t, σ_{cr}, σ_{tr} and both the elastic and softening moduli E, k_c, k_t. Since the elastic deformation is associated with friction sliding and progression of cracks, the elastic stiffness modulus may decrease in the course of deformation. Hence, it may be assumed that $E = E(\varepsilon^i)$, where ε^i denotes the irreversible portion of strain, Fig. 1b.

Consider first the case when the elastic stiffness modulus is constant and formulate the material stability and instability conditions. For the stable portion COA of the stress-strain curve, for any infinitesimal increment of stress and strain, there is

CA:

$$d\boldsymbol{\sigma}\cdot d\boldsymbol{\varepsilon}=d\boldsymbol{\sigma}\cdot d\boldsymbol{\varepsilon}^{e}+d\boldsymbol{\sigma}\cdot d\boldsymbol{\varepsilon}^{P}>0 \qquad \text{(stability)} \tag{1}$$

whereas for the unstable branches AB and CD, we have

AB or CD:

$$d\boldsymbol{\sigma}\cdot d\boldsymbol{\varepsilon}=d\boldsymbol{\sigma}\cdot d\boldsymbol{\varepsilon}^{e}+d\boldsymbol{\sigma}\cdot d\boldsymbol{\varepsilon}^{P}<0 \qquad \text{(instability)} \tag{2}$$

and the total strain increment is decomposed into elastic and plastic portions, thus $d\boldsymbol{\varepsilon}=d\boldsymbol{\varepsilon}^{e}+d\boldsymbol{\varepsilon}^{p}$. The usual small strain theory is applied and the dot between two vectors or tensors denotes their scalar product, thus $\boldsymbol{\sigma}\cdot\boldsymbol{\varepsilon}=\sigma_{ij}\,\varepsilon_{ij}$.

For finite stress and strain departures from the typical point S, the respective definition of stability is

$$U(\boldsymbol{\sigma}_T-\boldsymbol{\sigma}_S)=\int_{\boldsymbol{\varepsilon}_S}^{\boldsymbol{\varepsilon}_T}(\boldsymbol{\sigma}-\boldsymbol{\sigma}_S)\cdot d\boldsymbol{\varepsilon}>0 \qquad \text{(stability)} \tag{3}$$

and similarly for the departure from A on the unstable branch, we have

$$U(\boldsymbol{\sigma}_P-\boldsymbol{\sigma}_A)=\int_{\boldsymbol{\varepsilon}_A}^{\boldsymbol{\varepsilon}_P}(\boldsymbol{\sigma}-\boldsymbol{\sigma}_A)\cdot d\boldsymbol{\varepsilon}<0 \qquad \text{(instability)} \tag{4}$$

where $\boldsymbol{\sigma}_T$ and $\boldsymbol{\sigma}_P$ are the stress values on stable and unstable portions of the stress-strain diagram. Since for the elastic strain increments there is usually $d\boldsymbol{\sigma}\cdot d\boldsymbol{\varepsilon}^{e}>0$, the hardening (stability) and softening (instability) conditions can be expressed in terms of the plastic strain increment, namely

$$\text{hardening: } d\boldsymbol{\sigma}\cdot d\boldsymbol{\varepsilon}^{p}>0, \qquad \text{softening: } d\boldsymbol{\sigma}\cdot d\boldsymbol{\varepsilon}^{p}<0. \tag{5}$$

The inequalities (1)—(5) can easily be interpreted in the uniaxial case presented in Fig. 1. However, they can be applied as general definitions of stable and unstable material response for any stress state.

The increments $d\boldsymbol{\sigma}$ and $d\boldsymbol{\varepsilon}$ are interrelated by constitutive relations

$$d\boldsymbol{\sigma}=\mathrm{D}\,d\boldsymbol{\varepsilon}, \quad d\boldsymbol{\varepsilon}=\mathrm{C}\,d\boldsymbol{\sigma}, \quad \mathrm{C}=\mathrm{D}^{-1} \tag{6}$$

where the incremental stiffness and compliance matrices D and C depend in general on the stress state and the loading history. For an elastoplastic deformation process, such matrices depend on the type of hardening or softening rule and on the form of the yield condition. In the case, when the plastice deformation and brittle rupture process are accounted for, the respective constitutive matrices have been discussed, for instance, by Dragon and Mróz (1979).

For purely elastic strain increments, there is

$$d\boldsymbol{\sigma} \cdot d\boldsymbol{\varepsilon}^e = \mathbf{D}^e \, d\boldsymbol{\varepsilon}^e \cdot d\boldsymbol{\varepsilon}^e = \mathbf{C}^e \, d\boldsymbol{\sigma} \cdot d\boldsymbol{\sigma} = 2U \, (d\boldsymbol{\varepsilon}^e) > 0 \tag{7}$$

where $\mathbf{C}^e$ and $\mathbf{D}^e$ are elastic incremental compliance and stiffness matrices.

Consider now the stability conditions for any mining excavation shown schematically in Fig. 2. Assume the boundary conditions in displacements or in surface tractions to be specified on the portions S_u and S_T of the boundary and let the domain V occupied by rock be divided into two subdomains V_1 and V_2 where the subdomain V_1 is assumed to correspond to stable elastic or elasto-plastic behaviour satisfying (1) or (3) and the subdomain V_2 to be in the post-critical softening state satisfying (2) or (4). The state presented in Fig. 2 was attained in a quasistatic process of excavation which resulted in stress, strain and displacement redistribution from the initial state. This process is here controlled not by external loads or displacements but by geometric parameters such as a, d, specifying the configuration and size of excavation.

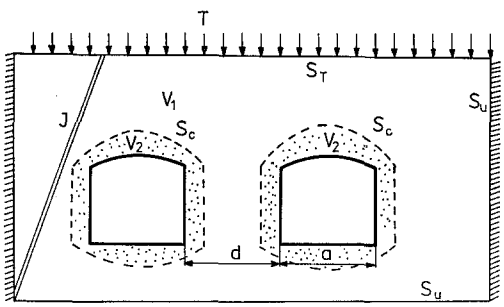

Fig. 2. Damaged zone V_2 around excavation within elastic rock

In order to examine the stability of a particular equilibrium configuration, let us introduce the *disturbance* into the system. This disturbance may be introduced in many ways but it always supplies the additional energy into the system. For instance, the disturbance can be thought of as an additional impulse imposing the velocity field within the domain such that the boundary conditions are satisfied. The disturbance can also be conceived as an additional field of body forces, surface tractions, boundary velocities acting over specified period of time or as a sudden removal of the stressed material element. In mining operations there are many disturbances resulting from dynamic deformation and burst of rock in neighbouring areas or from rock blasting. With each disturbance, the amount of energy supplied to the system can be associated, and the stability of subsequent motion will usually depend on this energy.

Consider now the disturbance in a form of the dynamic impulse superimposed at $t = t_0$ upon the equilibrium state, so that $\dot{\mathbf{u}}^0(x) = \mathbf{v}^0(x)$ within V

at $t=t_0$ and the kinetic energy of this impulse equals

$$\Delta K_0 = \int \frac{1}{2} \varrho \, \mathbf{v}^0 \cdot \mathbf{v}^0 \, dV \tag{8}$$

where ϱ denotes the material density. Denote the stress, strain and displacement fields at the initial equilibrium position by $\boldsymbol{\sigma}^0$, $\boldsymbol{\varepsilon}^0$ and $\mathbf{u}^0$. The subsequent values at $t > t_0$ are respectively

$$\boldsymbol{\sigma} = \boldsymbol{\sigma}^0 + \int_{t_0}^{t} \dot{\boldsymbol{\sigma}} \, d\tau, \quad \boldsymbol{\varepsilon} = \boldsymbol{\varepsilon}^0 + \int_{t_0}^{t} \dot{\boldsymbol{\varepsilon}} \, d\tau, \quad \mathbf{u} = \mathbf{u}^0 + \int_{t_0}^{t} \dot{\mathbf{u}} \, d\tau \tag{9}$$

and the subsequent motion is compatible with the boundary conditions on S_T and S_u, that is $\mathbf{T}^b = \boldsymbol{\sigma} \cdot \mathbf{n}$ on S_t and $\mathbf{u} = \mathbf{u}^b$ on S_u.

The increment of the elastic potential energy $\Delta \Pi_e$ and of the dissipated work ΔD equals

$$\begin{aligned}
\Delta \Pi_t = \Delta \Pi_e + \Delta D &= \int_{\boldsymbol{\varepsilon}^0}^{\boldsymbol{\varepsilon}} \int \boldsymbol{\sigma} \cdot d\boldsymbol{\varepsilon} \, dV - \int_{\mathbf{u}^0}^{\mathbf{u}} \int \mathbf{T}^b \cdot d\mathbf{u} \, dS_T - \int_{\mathbf{u}^0}^{\mathbf{u}} \int \mathbf{f} \cdot d\mathbf{u} \, dV = \\
&= \int_{\boldsymbol{\varepsilon}^0}^{\boldsymbol{\varepsilon}} \int (\boldsymbol{\sigma} - \boldsymbol{\sigma}^0) \cdot d\boldsymbol{\varepsilon} \, dV + \int_{\boldsymbol{\varepsilon}^0}^{\boldsymbol{\varepsilon}} \int \boldsymbol{\sigma}^0 \cdot d\boldsymbol{\varepsilon} \, dV - \int_{\mathbf{u}_0}^{\mathbf{u}} \int \mathbf{T}^b \cdot d\mathbf{u} \, dS_T - \int_{\mathbf{u}^0}^{\mathbf{u}} \int \mathbf{f} \cdot d\mathbf{u} \, dV = \\
&= \int_{\boldsymbol{\varepsilon}^0}^{\boldsymbol{\varepsilon}} \int (\boldsymbol{\sigma} - \boldsymbol{\sigma}^0) \cdot d\boldsymbol{\varepsilon} \, dV,
\end{aligned} \tag{10}$$

since by virtue of the virtual work principle for the stress state $\boldsymbol{\sigma}^0(x)$ satisfying equilibrium and boundary conditions and the kinematically admissible field $d\mathbf{u}$, $d\boldsymbol{\varepsilon}$, there is

$$\int \boldsymbol{\sigma}^0 \cdot d\boldsymbol{\varepsilon} \, dV = \int \mathbf{T}^b \cdot d\mathbf{u} \, dS_T + \int \mathbf{f} \cdot d\mathbf{u} \, dV. \tag{11}$$

Here $\mathbf{T}^b$ denotes the specified surface traction vector on the boundary portion S_T whereas $\mathbf{u}^b$ is the specified displacement vector on the portion S_u and $\mathbf{f}$ denotes the body force field. There is therefore $d\mathbf{u} = 0$ on S_u for the ensuing motion or for any kinematically admissible variation of the displacement field.

In view of the principle of conservation of energy, there is

$$\Delta K_0 = \Delta \Pi_t + \Delta K(t), \tag{12}$$

where $\Delta K(t)$ denotes the kinetic energy at any subsequent instant $t = t_0 + \Delta t$.

The *divergence instability* occurs when the kinetic energy of imposed motion will monotonically grow. To prevent this instability, the sufficient condition is

$$\Delta \Pi_t = \int_{\boldsymbol{\varepsilon}^0}^{\boldsymbol{\varepsilon}} \int (\boldsymbol{\sigma} - \boldsymbol{\sigma}^0) \cdot d\boldsymbol{\varepsilon} \, dV > 0 \tag{13}$$

for any kinematically admissible deformation path issuing from the equilibrium position. In fact, if $\Delta \Pi_t > 0$, then $\Delta K(t) < \Delta K_0$, and the system set in

motion with the initial kinetic energy ΔK_0 will come to rest after some time or will execute repetitive motion around the equilibrium position. Let us note that the integrand of (13) coincides with the integrand of (3) representing the material stability condition. For an infinitesimal departure from the equilibrium state along a regular path the condition (13) can be replaced by the incremental form

$$d\Pi_t = \frac{1}{2}\int d\boldsymbol{\sigma}\cdot d\boldsymbol{\varepsilon}\, dV = \frac{1}{2}\int d\boldsymbol{\sigma}\cdot d\boldsymbol{\varepsilon}^e\, dV + \frac{1}{2}\int d\boldsymbol{\sigma}\cdot d\boldsymbol{\varepsilon}^p\, dV > 0 \tag{14}$$

and it is obviously satisfied for a stable portion of the stress-strain curve.

Consider now the cyclic motion for which elastic unloading is followed by plastic deformation during successive motion reversals. For the k-th reversal, instead of (14), we now have

$$\Delta\Pi_t^{(k)} = \Delta\Pi_e^{(k)} + \sum_{i=1}^{k}\Delta D^{(i)} = \int U^{(k)}(d\boldsymbol{\varepsilon}^e)\, dV + \frac{1}{2}\sum_{i=1}^{k}\int (d\boldsymbol{\sigma}\cdot d\boldsymbol{\varepsilon}^p)^{(i)}\, dV \tag{15}$$

where $U^K(d\boldsymbol{\varepsilon}^e) = {}^1/_2\, D^e\, d\boldsymbol{\varepsilon}^e\cdot d\boldsymbol{\varepsilon}^e$ is the elastic specific incremental energy that may grow or decrease during the cyclic motion, whereas the second irreversible term represents the accumulated incremental plastic work. Assume that $d\boldsymbol{\sigma}\cdot d\boldsymbol{\varepsilon}^p < 0$, that is the softening response occurs for each incremental plastic flow. Since the maximum value of $\Delta\Pi_t$ equals ΔK_0, then in view of (15), the amplitude of elastic strain must grow in consecutive portions of motion, that is

$$\Delta\Pi_e^{(k)} > \Delta\Pi_e^{(k-1)}. \tag{16}$$

Thus, there exists a possibility of *cyclic instability* for which the amplitude of superposed motion will grow due to repetitive plastic flow during each cycle. This model resembles much the flatter instability occurring in aeronautical structures due to non-conservative loading of the airstream. Figs. 3 b, c present schematically these two mechanisms of instability in the phase plane $(\mathbf{u}, \dot{\mathbf{u}})$, where $\mathbf{u}$ denotes the displacement of a typical point within the rock mass. It can also be conceived that a *combined mode* of instability will occur when after several cycles, the condition (13) or (14) is violated and the subsequent motion ensues with the unbounded kinetic energy, Fig. 3 d. The activating energy for cyclic instability modes can be provided by waves reflected on inhomogeneities or rock layer interfaces.

Consider now the case when besides the region V_2 with a continuously varying displacement field, there exist isolated joint surfaces S_d where discontinuities in displacements are related to contact tractions in a form of the incremental law

$$\begin{bmatrix} d\,T_n \\ d\,T_t \end{bmatrix} = \begin{bmatrix} A_{nn} & A_{nt} \\ A_{tn} & A_{tt} \end{bmatrix} \begin{bmatrix} d\,\bar{u}_n \\ d\,\bar{u}_t \end{bmatrix} \tag{17}$$

where $d\bar{u}_n$, $d\bar{u}_t$ are the increments of normal and tangential discontinuity components and dT_n, dT_t are the increments of contact tractions on S_d.

Similarly to (14), for the softening response we have

$$d\mathbf{T}\cdot d\bar{\mathbf{u}}=dT_n\cdot d\bar{u}_n+dT_t\cdot d\bar{u}_t<0. \tag{18}$$

The stability condition (14) now takes the form

$$\frac{1}{2}\int d\boldsymbol{\sigma}\cdot d\boldsymbol{\varepsilon}\,dV+\frac{1}{2}\int d\mathbf{T}\cdot d\bar{\mathbf{u}}\,dS_j>0 \tag{19}$$

where S_j denotes the area of the joint surface.

So far, we have discussed the perturbation imposed by a dynamic impulse within the specified domain. However, similar stability conditions are obtained by considering perturbation of surface tractions or of surface

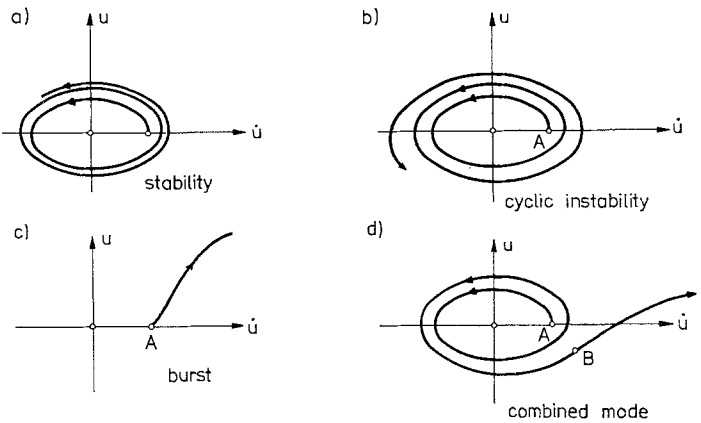

Fig. 3. Possible modes of dynamic instability

displacements on boundary portions S_T or S_u. Assume that the traction increment $d\mathbf{T}^0$ is superposed during the time interval (t_0, t_1) on S_T and removed for $t>t_1$. Instead of (12), we now have

$$\Delta W_0=\int d\mathbf{T}^0\cdot d\mathbf{u}^0\,dS_T=\int_{t_0}^{t}\int(\boldsymbol{\sigma}-\boldsymbol{\sigma}^0)\cdot\dot{\boldsymbol{\varepsilon}}\,dt\,dV+\Delta K \tag{20}$$

where $d\mathbf{u}^0$ denotes the displacement increment during the time period (t_0, t_1). The identical inequality is obtained by imposing constant velocity perturbation on S_u during the time interval (t_0, t_1). The left-hand side of (20) can now be regarded as the incremental work ΔW_0 of surface perturbation and it can be used as a measure of intensity of perturbation, similarly as the kinetic energy ΔK_0 in (12).

The stability condition can also be expressed in an alternative form equivalent to (14). Consider separately the subdomains V_1 and V_2 and assume that the interface S_c separating these subdomains has attained an imposed displacement variation $\delta\mathbf{u}^c$. Consider static solutions associated with

this variation in V_1 and V_2, that is the fields $\delta\boldsymbol{\sigma}^{(1)}$, $\delta\mathbf{u}^{(1)}$, $\delta\boldsymbol{\varepsilon}^{(1)}$ and $\delta\boldsymbol{\sigma}^{(2)}$, $\delta\mathbf{u}^{(2)}$, $\delta\boldsymbol{\varepsilon}^{(2)}$ satisfying equilibrium, compatibility and boundary conditions on S_T and S_u, namely

$$\delta\sigma_{ij,j}=0 \quad \text{within } V, \qquad \delta\sigma_{ij}n_j=0 \quad \text{on } S_T, \qquad \delta\mathbf{u}=0 \quad \text{on } S_u,$$
$$\delta\mathbf{u}=\delta\mathbf{u}^c \quad \text{on } S_c. \tag{21}$$

The stability condition (14) can now be expressed as follows

$$\int \delta\boldsymbol{\sigma}\cdot\delta\boldsymbol{\varepsilon}\, dV = \int (\delta\mathbf{T}^{(2)}-\delta\mathbf{T}^{(1)})\cdot\delta\mathbf{u}^c\, dS_c > 0 \tag{22}$$

where $\delta\mathbf{T}^{(1)}=-\delta\boldsymbol{\sigma}^{(1)}\cdot\mathbf{n}_c$, $\delta\mathbf{T}^{(2)}=\delta\boldsymbol{\sigma}^{(2)}\cdot\mathbf{n}_c$ and $\mathbf{n}_c$ is the unit normal vector to S_c directed into the domain V_1. This form of stability condition was analysed by Petukchov and Linkov (1979) and applied by Salamon (1970) to study stability of a set of pillars. The instability condition is obtained by changing the inequality sign in (22).

There is a simple geometrical visualization of the condition (22) in the case when $\delta\mathbf{u}^c=\delta u^c\mathbf{n}_c$ where u^c is the constant modulus and $\mathbf{n}_c$ is the unit vector. Then $\delta\mathbf{T}\cdot\delta\mathbf{u}^c=\delta T_u\delta\mathbf{u}_c$ where δT_u is the component of traction variation along u_c. The instability condition is then expressed as follows

$$(\delta\bar{T}^{(2)}-\delta\bar{T}^{(1)})\cdot\delta u^c<0 \tag{23}$$

where

$$\delta\bar{T}^{(1)}=\int\delta T_u{}^{(1)}\, dS_c, \qquad \delta\bar{T}^{(2)}=\int\delta\bar{T}_u{}^{(2)}\, dS_c \tag{24}$$

are the integrated traction variations δT_u over the surface S_c. Plotting $\bar{T}^{(1)}$ and $\bar{T}^{(2)}$ versus u^c for specified boundary conditions depending on one loading or displacement parameter, the equilibrium curve $\bar{T}^{(1)}(u^c)=\bar{T}^{(2)}(u^c)$ is obtained corresponding to variation of this parameter, Fig. 4. Imposing now variation $\delta\mathbf{u}^c$ on S_c and constructing solutions in V_2 and V_1 satisfying (20), that is corresponding to a fixed value of loading parameter, the instability occurs when the $\delta T^{(1)}$-line lies above the $\delta T^{(2)}$-line, cf. point B in Fig. 4.

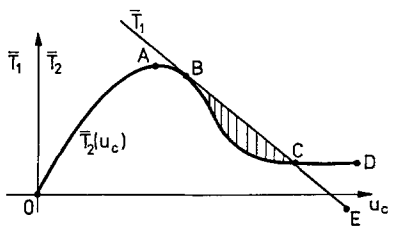

Fig. 4. Determination of static instability point B

For monotonically growing δu^c, the equilibrium lines for V_1 and V_2 are now BCD and BCE and the dynamic deformation process may occur starting from the limit equilibrium point B.

The energy of burst associated with the dynamic process can be measured by the integral

$$E_t = \int_0^{\mathbf{u}_r} \int (\mathbf{T}^{(1)} - \mathbf{T}^{(2)}) \cdot d\,\mathbf{u}^c \, dS_c = \int_0^{\boldsymbol{\varepsilon}_r} \int (\boldsymbol{\sigma} - \boldsymbol{\sigma}_B) \cdot d\,\boldsymbol{\varepsilon} \, dV \tag{25}$$

represented by the dashed area in Fig. 4. Here $\mathbf{u}_r$ and $\boldsymbol{\varepsilon}_r$ denote the displacement and strain at the equilibrium point C where $T^{(1)} = T^{(2)}$. A more detailed discussion of dynamic failure modes in simpler simulation hyperstatic systems will be presented by the authors in a separate paper, where the importance of E_t is explored. In the next section, we shall present a numerical approach to study rock burst processes treated as problems of dynamic instability.

3. Numerical Simulation of Rock Burst Processes

Consider a mining excavation shown in Fig. 2 and a sufficiently large domain of a surrounding rock mass. Assume that static solution has been determined for a specified configuration. This solution may correspond to elastic or elasto-plastic state. The incremental process can be conceived in which the size of the excavation is step-by-step increased until the instability point is reached. Using the finite element discretization, we can write

$$\mathbf{K}\, d\boldsymbol{\delta} = \delta \mathbf{F} \tag{26}$$

where $\mathbf{K}$ denotes the global stiffness matrix, $d\boldsymbol{\delta}$ are the increments of nodal displacements and $d\mathbf{F}$ are the increments of nodal forces. At each step of the variation of excavation size, a new incremental solution is obtained. The instability point is then specified by the condition

$$\det [\mathbf{K}] = 0 \tag{27}$$

or

$$\int d\boldsymbol{\sigma} \cdot d\boldsymbol{\varepsilon} \, dV = 0. \tag{28}$$

The condition (27) was applied in determining instability point by static analysis but it turned out that variation of det [K] becomes vary rapid close to instability point and very small increments of excavation dimensions should be taken. This makes the procedure very lengthy and expensive from the point of view of computer cost. Furthermore, there is no information on post-critical behaviour and on failure mode since the static solution procedure terminates at the instability point.

The dynamic approach was therefore considered as more natural and economic, providing information not only on the onset of instability but also on the whole dynamic failure process. Instead of static equilibrium equations (26), consider now the equations of motion

$$\mathbf{K}\boldsymbol{\delta} + \mathbf{C}_d \dot{\boldsymbol{\delta}} + M \ddot{\boldsymbol{\delta}} = \mathbf{F}(t) \tag{29}$$

where $\mathbf{K}$ denotes the stiffness matrix, $\mathbf{C}_d$ is the damping matrix and $\mathbf{M}$ is

the mass matrix. The static solution is first obtained for a specified configuration and within the elastic-plastic range this solution is constructed incrementally by imposing small variations in excavation dimensions. At some stage, a small dynamic disturbance is introduced into the system. This may be achieved by specifying either initial velocity field $\mathbf{v}_0(\mathbf{x})$ of prescribed total kinetic energy K_0 or by initiating a dynamic process by sudden removal of portions of rock, which may be compared to step loading in structural mechanics. The subsequent dynamic solution will indicate whether growth of the kinetic energy occurs within the system, and if so, the associated failure mode can be investigated. If, however, the initial disturbance is not amplified, a further increase in excavation dimension may be imposed and the corresponding static solution may be constructed. Alternatively, a greater dynamic disturbance may be imposed until the unstable process occurs. Fig. 5 a, b illustrates schematically this procedure in the $P-u$ diagram where P is the external load and u is the associated displacement. After constructing static solution at 1, the dynamic impulse is imparted to a structure of kinetic energy K_0 which is greater than the dashed area 1-A-2 in Fig. 5 a. Under fixed value of P, the ensuing dynamic process 1—2 passes through the stable domain 1-A-2 and enters the unstable domain in which

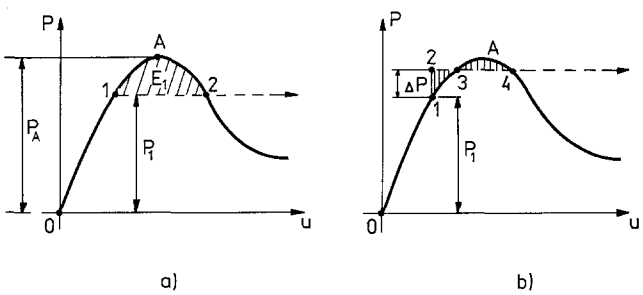

Fig. 5. Dynamic instability; applying at 1
a) initial impulse of the kinetic energy $K_0 > E_1$ or b) step loading ΔP, the subsequent motion under fixed value of P proceeds into unstable domain

further growth of kinetic energy and of displacement occurs until the second equilibrium point is reached. Fig. 5 b presents the situation when a step loading ΔP is applied at 1, such that the area 1-2-3 is greater than the area 3-A-4. The corresponding dynamic process 2-3-4 passes into unstable domain though the total load $P_1+\Delta P$ is smaller than the maximal load P_A.

3.1 Finite-Element Discretization

In carrying out dynamic analysis of rock, any finite element discretization can be applied. However, it was found out that this analysis is considerably simplified when special rigid elements are used and both elastic and plastic properties are lumped into a set of *interaction nodes* lying on element interfaces. It can be conceived that the adjacent elements are inter-

connected at these nodes by a set of tangential and normal springs whose forces are related to relative displacements of adjacent nodes.

Referring to Fig. 6, consider a set of rectangular rigid blocks whose mass is lumped at their centres. The motion of each block and its position are specified by translation vector, rotation angle and their rates at its centre, u_x, u_y, ω and $\dot{u}_x$, $\dot{u}_y$, $\dot{\omega}$. We limit our analysis to plane deformation,

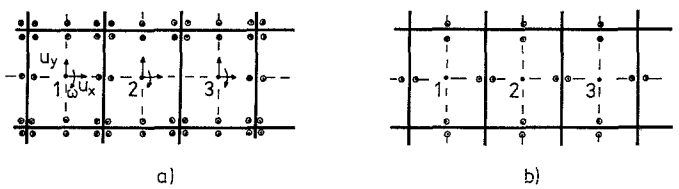

Fig. 6. Contact finite elements interacting through side and corner nodes: a) elastic interaction; b) post-critical frictional interaction

so the nodal displacement vector for each block $\boldsymbol{\delta}^i$ $(u_x{}^i, u_y{}^i, \omega^i)$ is referred only to the *configuration node* (centre) and is specified by three components. The displacement of the typical interaction node D between two elements equals

$$\begin{aligned} \mathbf{u}_D{}^i &= \mathbf{u}^i + \boldsymbol{\omega}^i \wedge (\mathbf{r}_D - \mathbf{r}_0{}^i), \\ \mathbf{u}_D{}^j &= \mathbf{u}^j + \boldsymbol{\omega}^j \wedge (\mathbf{r}_D - \mathbf{r}_0{}^j), \end{aligned} \tag{30}$$

and the relative displacement at the interaction node equals

$$\boldsymbol{\delta}_D = \mathbf{u}_D{}^j - \mathbf{u}_D{}^i \tag{31}$$

where $\mathbf{r}_0{}^i$ and $\mathbf{r}_0{}^j$ are position vectors of configuration nodes of two elements i and j, $\mathbf{r}_D$ is the position vector of the interaction node D, $\mathbf{u}^i$, $\mathbf{u}^j$, $\boldsymbol{\omega}^i$ and $\boldsymbol{\omega}^j$ are the translation vectors and rotation angles at the configuration nodes, and the symbol $\wedge$ denotes the vector product. Decomposing $\boldsymbol{\delta}_D$ into normal and tangential components δ_{nD} and δ_{tD}, the elastic energy at each interaction node is expressed as follows

$$U_d = \frac{1}{2}\,(K_n\,\delta_{nD}{}^2 + K_t\,\delta_{tD}{}^2) \tag{32}$$

where K_n, and K_t are the normal and tangential node stiffness. Summing up the elastic energies at all interaction nodes and using (30), the total elastic energy of the system can be expressed in terms of the nodal displacements $\boldsymbol{\delta}^i$, that is

$$U_t = \frac{1}{2}\,\boldsymbol{\delta}^T \cdot \mathbf{K}\boldsymbol{\delta} \tag{33}$$

where $\mathbf{K}$ denotes the global stiffness matrix. The static equilibrium equations $\mathbf{K}\boldsymbol{\delta} = \mathbf{F}$ or the equations of motion (27) can now be generated in a standard way.

The stiffness parameters K_n, K_t at the interaction nodes are next identified by requiring that the response of a representative macroelement composed of contact finite elements under uniform external strain, for instance, tension and shear, should correspond to actual response of the material. It turns out that in some cases the initial prestress at interaction nodes represented by an additional nodal force $\mathbf{F}^i$ produces a considerable improvement in simulation. For instance, the lateral expansion of a compressed isotropic bar is well simulated by a set of rectangular elements when the initial prestress is introduced in lateral direction at the nodes, thus inducing the equilibrium equation $\mathbf{K}\boldsymbol{\delta}=\mathbf{F}+\mathbf{F}^i$. Details of identification will be omitted here and are presented by Zubelewicz (1982).

Let us now discuss the plastic behaviour which is also lumped at the interaction nodes. Assume that the material satisfies a modified Coulomb criterion in which limit tension cut-off planes are introduced, Fig. 7 a. In terms of principal stresses this condition is expressed as follows

$$\begin{aligned} f_1(\sigma) &= \frac{1}{2}(\sigma_2-\sigma_1)+\frac{1}{2}(\sigma_1+\sigma_2)\sin\varphi - c\cos\varphi = 0, \quad (\sigma_2>\sigma_1) \\ f_2(\sigma) &= \frac{1}{2}(\sigma_1-\sigma_2)+\frac{1}{2}(\sigma_1+\sigma_2)\sin\varphi - c\cos\varphi = 0, \quad (\sigma_1>\sigma_2) \\ f_3(\sigma) &= \sigma_1-\sigma_r = 0, \\ f_4(\sigma) &= \sigma_2-\sigma_r = 0, \end{aligned} \tag{34}$$

where c and φ denote the cohesion and the angle of friction for the Coulomb material, whereas σ_r is the rupture stress in tension. As the stress state within the element is not homogeneous, the mean stress components are

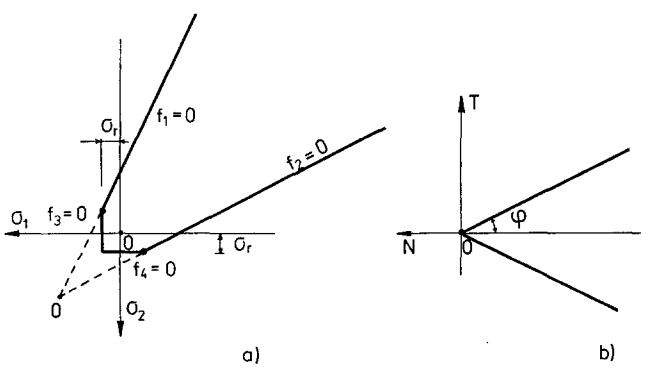

Fig. 7. a) Initial failure locus; b) post-critical contact gliding locus

calculated within each quarter of the element, assuming linear distribution of contact stresses at the interfaces. Once the limit condition (34) is satisfied, within a typical quarter-element, the rupture of the adjacent corner springs is assumed to occur and the subsequent interaction occurs only at

the remaining mid-side nodes. The limit contact condition for these nodes takes the form, Fig. 7b,

$$f(T, N) = T + \mu N = 0 \tag{35}$$

where μ denotes the contact friction coefficient, not necessarily equal to $\operatorname{tg}\varphi$. Thus, whereas (34) corresponds to brittle rupture of springs of corner nodes, (35) represents the subsequent post-critical response. The normal and tangential displacement increments at interfaces are governed by the relations

$$du_n = du_n^e + du_n^p, \quad du_t = du_t^e + du_t^p, \tag{36}$$

and

$$du_n^e = \frac{dN}{K_n}, \quad du_n^p = 0, \quad du_t^e = \frac{dT}{K_t}, \quad du_t^p = d\lambda \operatorname{sgn}(T) \tag{37}$$

where K_n and K_t are the elastic stiffness moduli of nodal springs and $d\lambda$ is an unspecified positive multiplier. Let us note that the limit condition (34) is expressed in terms of stresses rather than contact forces as it describes the limit state within a particular quarter-element. However, this condition can also be expressed directly in terms of nodal forces.

3.2 *Example 1: Dynamic Rupture of Rock Pillars*

Consider a mining excavation shown in Fig. 8, with three rooms and two pillars at the depth $h_b = 824$ m. As only the region in the vicinity of excavation is considered, it is assumed that the upper neglected rock domain exerts a vertical pressure $\sigma_y = \gamma h_t = -16.36$ MPa at the depth $h_t = 800$ m, corresponding to the top confining surface. At the vertical confining surfaces the horizontal displacements u_x are assumed to vanish whereas at the bottom horizontal surface passing through symmetry centers of rooms and pillars the vertical displacement u_y is assumed to vanish. The solution domain is therefore limited to the upper portion of pillars and the adjacent rock.

The solution procedure consisted of two stages. First, the static solution was found for the assumed initial configuration of rooms and pillars. Next, the dynamic solution was determined by assuming subsequent sudden removal of particular elements of pillar I. The dynamic instability of the configuration was detected by studying variation of the kinetic energy within the solution domain.

The solution domain was divided into 189 rectangular elements assuming plane-strain conditions, Fig. 8. Elastic properties of rock mass were assumed as follows: $E = 51.19$ GPa, $\nu = 0.27$ and the specific weight was assumed as $\gamma = 19.6$ kN/m^3. The material parameters occuring in the limit condition (34) are: $c = 24.5$ MPa, $\varphi = 27^0$, $\mu = \operatorname{tg}\varphi$, and $\sigma_c = 3.92$ MPa. The static solution was compared with the respective solution obtained for a standard finite-element mesh using the constant-strain triangular elements. This comparison enabled us to introduce proper correction to the stiffness matrix and to the horizontal forces f_s introduced at the nodes 1—9 and 181—189.

The explicit integration method was applied in integrating dynamic Eqs. (29) in which the viscous damping was neglected, $C_{\alpha}=0$. The time step was assumed as $\Delta t=0.2156\cdot 10^{-4}$ secs and the elements 63, 62, and 72, 71

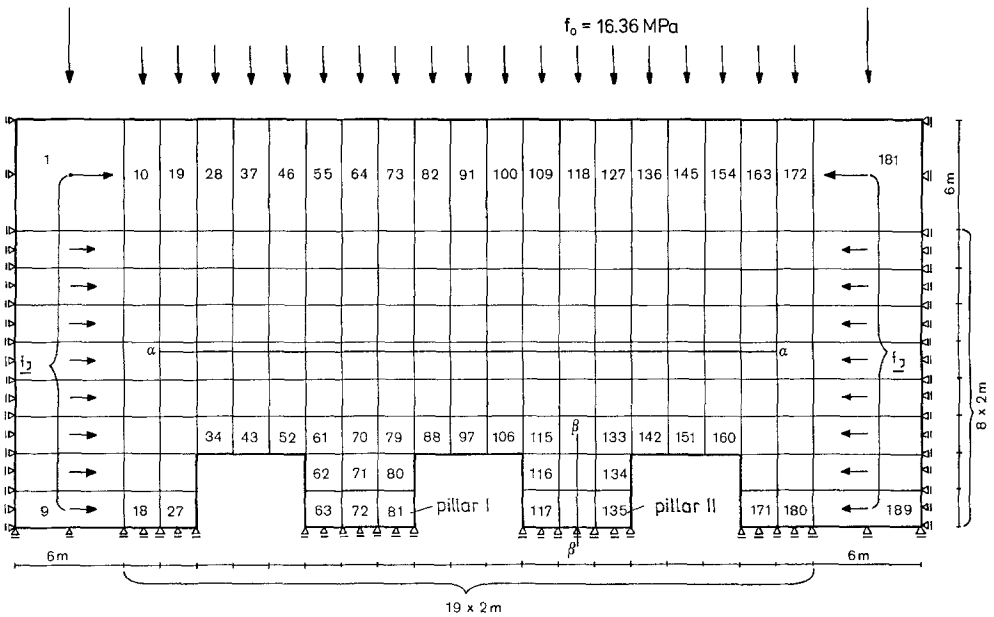

Fig. 8. Mining excavation with consecutive removal of pillar I

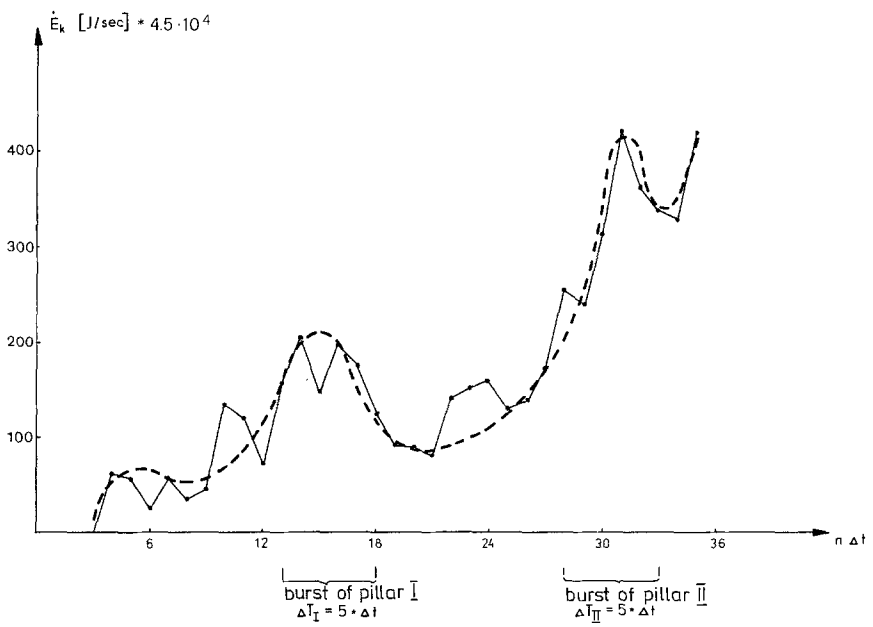

Fig. 9. Variation of the rate of kinetic energy $\dot{E}_k$ within the solution domain

of pillar I were consecutively removed at time steps equal to $3\,\Delta t$. The central difference scheme was applied and the stability condition $\Delta t \leq \frac{2}{\omega_{\max}}$ is satisfied by this step. Here, $\omega_{\max}$ is the maximum eigen-frequency of elements including interacting springs. Fig. 9 presents the rate of kinetic energy variation within the solution domain for consecutive time steps. It can be expected that rapid growth of $\dot{E}_k$ is associated with the phenomenon of dynamic rock failure. In fact, after removal of 2/3 of pillar I, the ensuing dynamic process is associated with the failure of remaining portion of pillar I and subsequently, the failure of pillar II proceeds which is manifested by the second rapid growth of $\dot{E}_k$, Fig. 9. The pillar failure is accompanied by the intense cracking of roof rock and its fall into excavated domain. The calculation process was terminated at $t_k = 36\,\Delta t$.

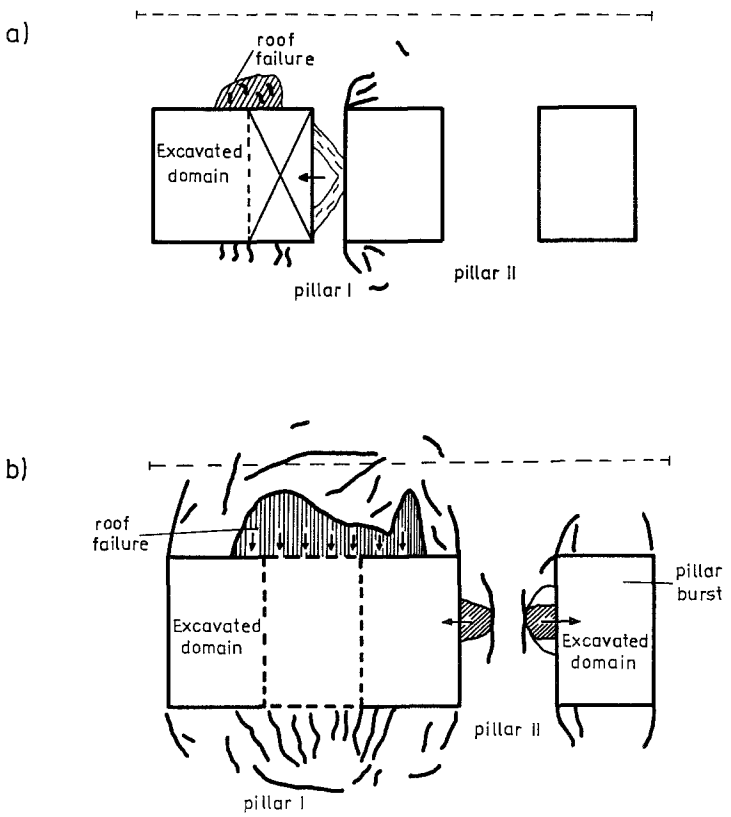

Fig. 10. Failure modes of a) pillar I, and b) pillar II accompanied by roof failure

Figs. 10 a, b illustrate schematically the failure mode at $t_1 = t_0 + 21\,\Delta t$ and $t = t_0 + t_k = t_0 + 36\,\Delta t$. Whereas for $t = t_1$ the remaining portion of pillar I undergoes dynamic failure and intense cracking occurs within the roof domain, for $t = t_k$ the pillar II has failed due to tensile stresses in horizontal

direction and a significant portion of roof rock is falling into the excavated domain. Fig. 11 shows the evolution of stress σ_x at the mid-section $\beta-\beta$ of pillar II. It is seen that at some instant the horizontal normal stress attains

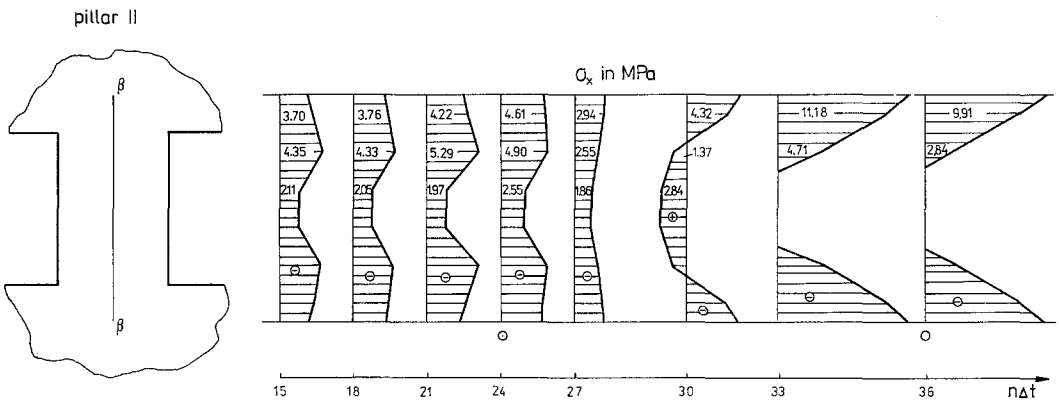

Fig. 11. Evaluation of the horizontal stress σ_x acting in the mid-section $\beta-\beta$ of pillar II

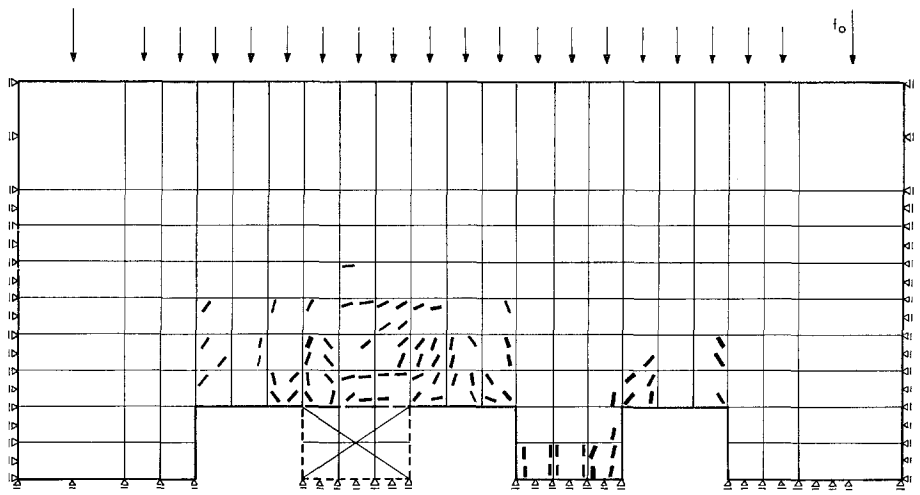

Fig. 12. Crack orientation within the rock mass at $t=t_k$

the rupture stress σ_r and the vertical crack propagates within the pillar. Fig. 12 shows the orientation of cracks within the rock mass at $t=t_k$.

3.3 *Example 2: Dynamic Failure of the Excavation Face Initiated by Plane Wave*

Consider a rock mass shown in Fig. 13. The initial static state is obtained by imposing vertical and horizontal displacements $u_y{}^0=1.0$ cm and $u_x{}^0=0.5$ cm at upper horizontal and left vertical boundaries. The bottom

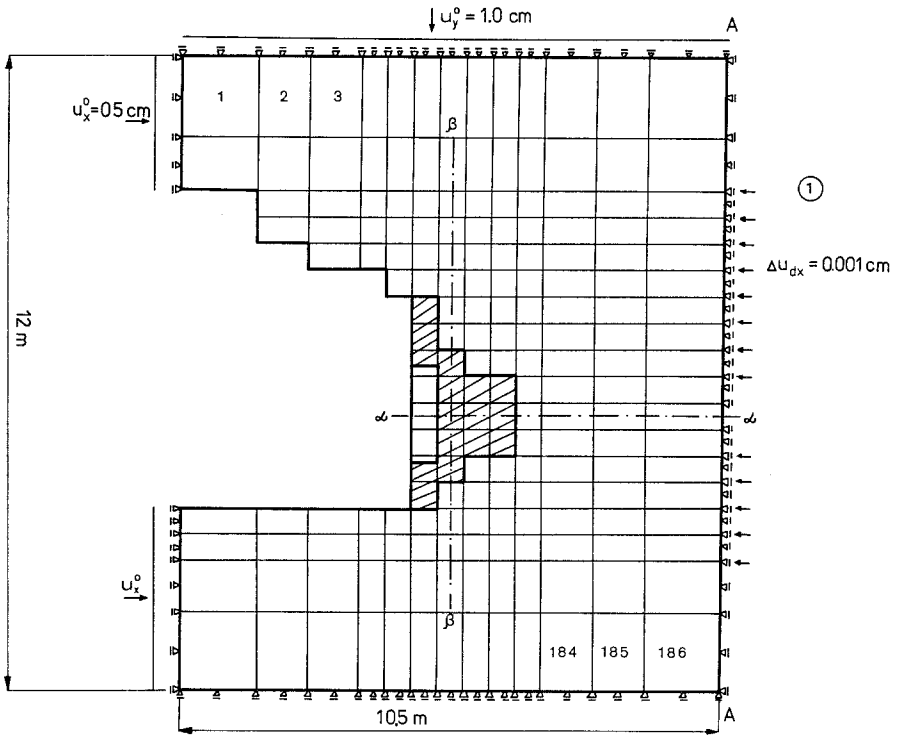

Fig. 13. Excavation face under initial static stress and acted on by plane dynamic disturbance on the boundary A – A

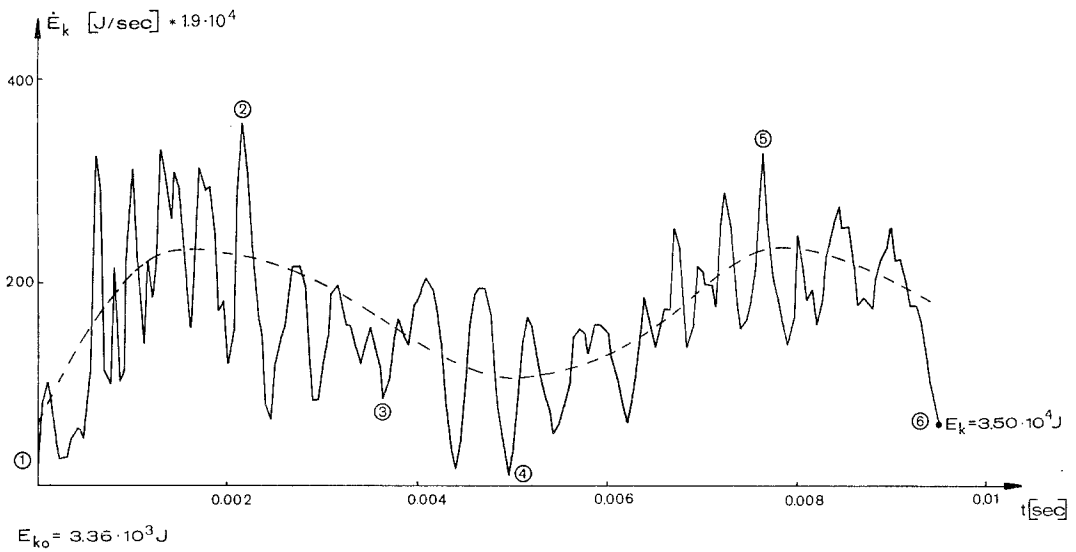

Fig. 14. Variation of the rate of kinetic energy $\dot{E}_k$ within the solution domain

boundary is vertically constrained whereas the right vertical boundary is horizontally constrained. The elastic material parameters are $E=15.7$ GPa, $\nu=0.12$ whereas the strength parameters are $c=31.4$ MPa, $\sigma_r=1.57$ MPa,

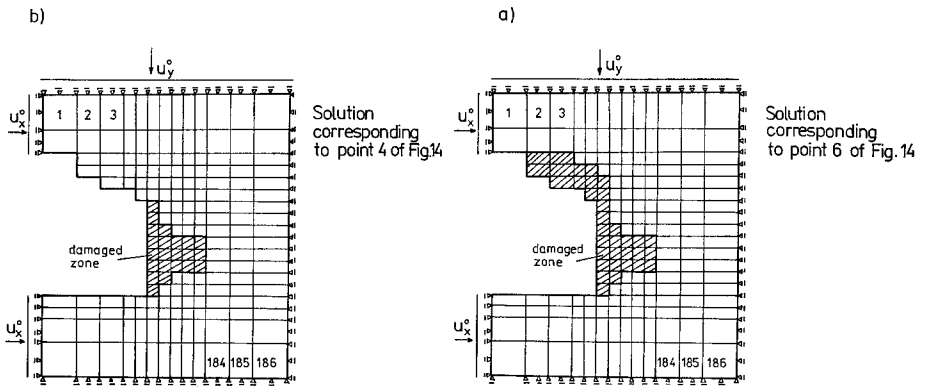

Fig. 15. Damaged zones within the rock mass at instants 4 and 6, marked in Fig. 14

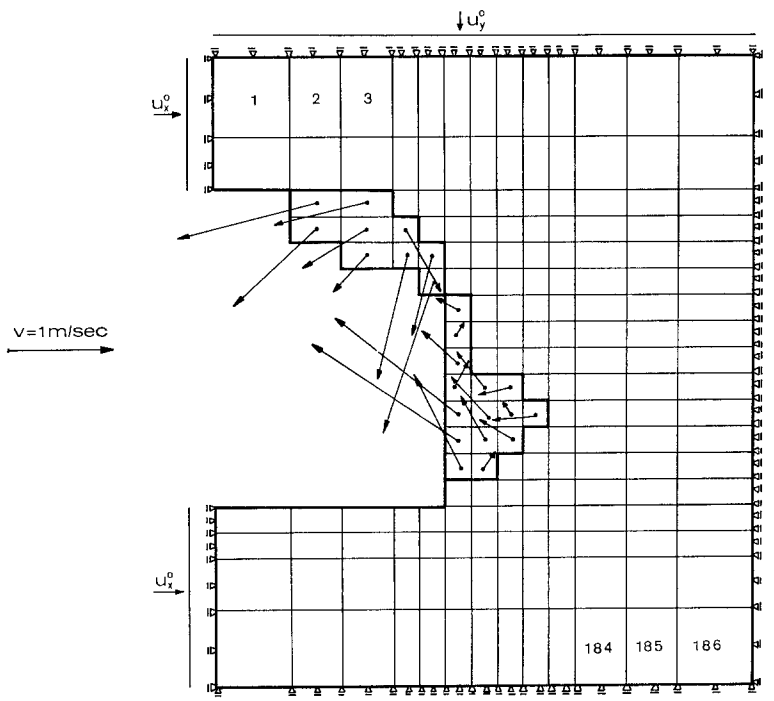

Fig. 16. Velocity field within the damaged portion of rock at instant 6 marked in Fig. 14

tg $\varphi=\mu=0.2$. At the initial instant $t=t_0$, the horizontal dynamic disturbance is applied at the right boundary $A-A$, by imposing the compressive displacement increment $\Delta u_{dx}=0.001$ cm in one time step $\Delta t=0.53\cdot 10^{-4}$ secs.

The subsequent dynamic process is studied and the variation of the kinetic energy rate within the solution domain is shown in Fig. 14. Whereas the initial kinetic energy was equal to $E_k = 3.36 \cdot 10^3$ J, the value of E_k after time interval 0.01 sec was equal to $E_k = 3.50 \cdot 10^4$ J.

Figs. 15 a, b show the damaged zones within the rock mass at point 4 and 6 marked in Fig. 14. Due to tensile action the fractured rock is disintegrated and is thrown into the excavation domain. Fig. 16 illustrates the velocity field within the damaged portion of rock.

The present example can be referred to a situation occurring at the rock face when the incoming plane wave produces dynamic failure and ejection of damaged material into the excavated room.

3.4 Example 3: Burst of Inhomogeneous Rock Into the Tunnel

Consider a horizontal rectangular tunnel within the inhomogeneous rock mass. The stiff rock ($E = 50$ GPa) is separated from soft rock ($E = 5$ GPa) by a horizontal layer of intermediate stiffness ($E = 20$ GPa). The floor of the excavated tunnel coincides with the interface between the layer and the stiff rock (Fig. 17). Consider the solution domain shown in Fig. 18,

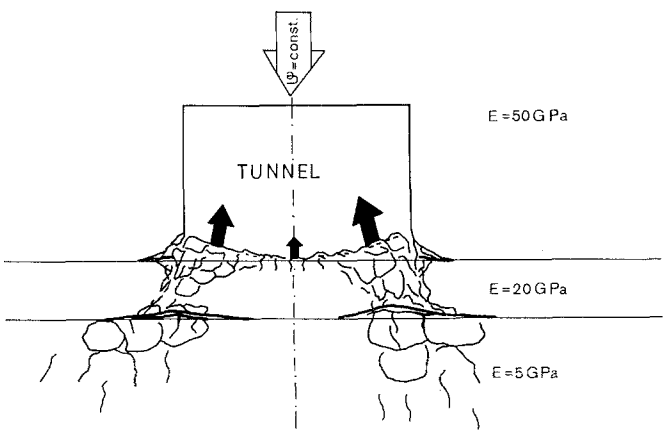

Fig. 17. Horizontal tunnel within the inhomogeneous rock mass. The dynamic failure mode

where the initial static state corresponds to non-uniform vertical stress σ_y applied at the upper boundary and horizontal displacement $u_x = 0.5$ cm at right vertical boundary, whereas the bottom boundary is constrained. Consider the vertically moving dynamic disturbance $v_{dy} = 0.0075$ cm/sec applied at the top boundary. The subsequent dynamic solution exhibits the rupture mode. Fig. 19 shows the variation of $\dot{E}_k$ whereas Figs. 20 a, b, c show the progression of damaged zones. The mode of failure is schematically depicted in Fig. 17. Due to tensile action, the delamination between the layer and the soft rock occurs with the associated energy release and rupture of the layer. The damaged material is pushed into the tunnel exhibiting the familiar effect of floor burst.

4. Concluding Remarks

The presented examples illustrate clearly the main idea of this paper, namely: by solving initial static and subsequent dynamic problems, the dynamic mode of failure can be numerically studied for any specified configuration and initial conditions. Moreover, the onset of dynamic failure mode

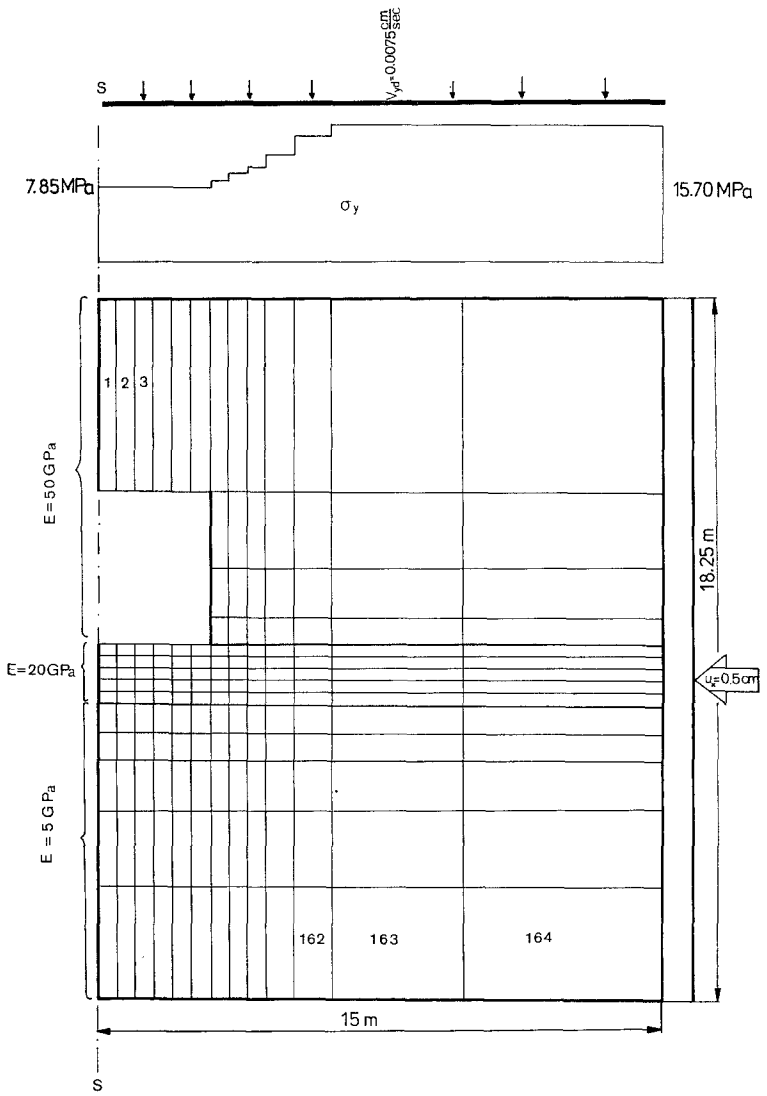

Fig. 18. The solution domain and finite element mesh

can be determined by studying the variation of the kinetic energy rate within the solution domain. The application of contact finite elements simplifies the analysis and allows for disintegration of particular rock elements.

It is believed that the approach presented provides the possibility for systematic quantitative analysis of rock burst phenomena. Further applications to study typical burst modes will be presented in a future.

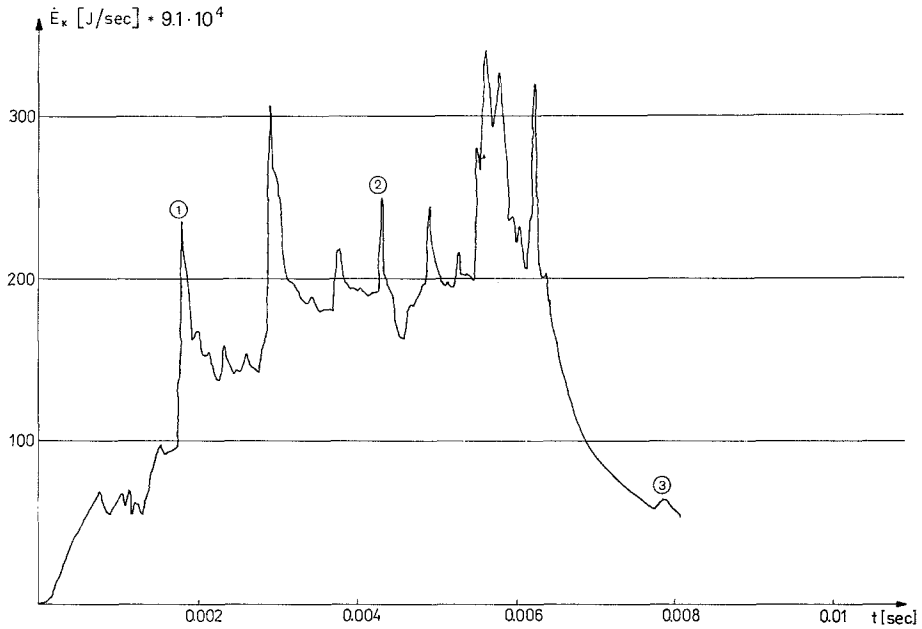

Fig. 19. The variation of $\dot{E}_k$ within the solution domain

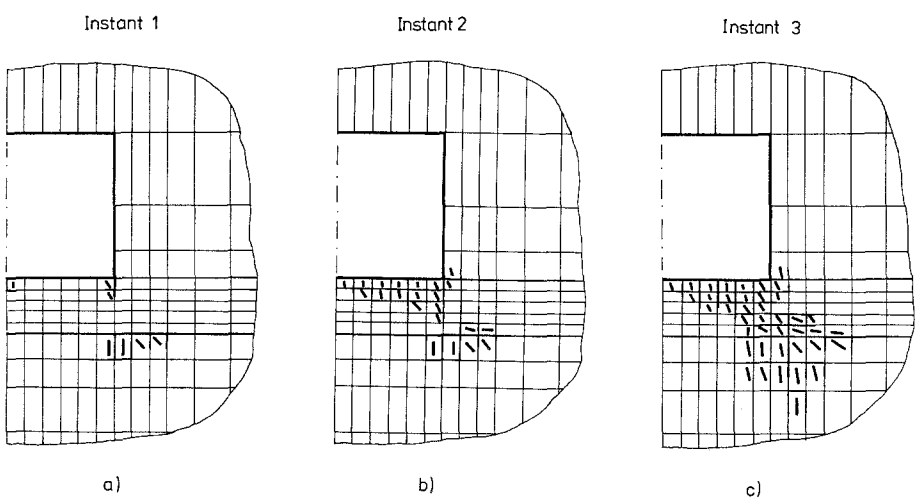

Fig. 20. Progression of damage: cracked domains at instants 1, 2 and 3 marked in Fig. 19

References

Bieniawski, Z. T. (1968): Fracture Dynamics of Rock. Int. J. Fract. Mech., Vol. 4, 415—430.

Burgert, W., Lippmann, H. (1981): Models of Translatory Rock Bursting in Coal. Int. J. Rock Mech. Min. Sci. and Geom. Abstr., Vol. 18, 285—294.

Crouch, S. L., Fairhurst, C. (1974): Mechanics of Coal Mine Bumps. Trans. Am. Inst. Min. Engrs., Vol. 256, 317—323.

Dragon, A., Mróz, Z. (1979): A Continuum Model for Plastic-Brittle Behaviour of Rock and Concrete. Int. J. Eng. Sci., Vol. 17, 121—137.

Mróz, Z., Zubelewicz, A. (to be published): On Dynamic Modes of Failure of Brittle-Plastic Structures. Arch. Mech.

Petukchov, I. M., Linkov, A. M. (1979): The Theory of Post-Failure Deformations and the Problem of Stability in Rock Mechanics. Int. J. Rock Mech. Min. Sci. and Geom. Abstr., Vol 16, 57—76.

Salamon, M. D. G. (1970): Stability, Instability and Design of Pillar Workings. Int. J. Rock Mech. Min. Sci., Vol. 7, 613—631.

Zubelewicz, A. (1982): On Application of Contact Finite Elements in Solving Elasto-Plastic Problems. IPPT-Rep.